Density-matrix renormalization group study of the extended Kitaev-Heisenberg model

Kazuya Shinjo,[1,2,*] Shigetoshi Sota,[3] and Takami Tohyama[4]

[1]*Yukawa Institute for Theoretical Physics, Kyoto University, Kyoto 606-8502, Japan*

[2]*Computational Condensed Matter Physics Laboratory, RIKEN, Saitama 351-0198, Japan*

[3]*Computational Materials Science Research Team, RIKEN AICS, Hyogo 650-0047, Japan*

[4]*Department of Applied Physics, Tokyo University of Science, Tokyo 125-8585, Japan*

(Received 17 October 2014; revised manuscript received 9 January 2015; published 4 February 2015)

We study an extended Kitaev-Heisenberg model including additional anisotropic couplings by using the two-dimensional density-matrix renormalization group method. Calculating the ground-state energy, entanglement entropy, and spin-spin correlation functions, we make a phase diagram of the extended Kitaev-Heisenberg model around the spin-liquid phase. We find a zigzag antiferromagnetic phase, a ferromagnetic phase, a 120° antiferromagnetic phase, and two kinds of incommensurate phases around the Kitaev spin-liquid phase. Furthermore, we study the entanglement spectrum of the model, and we find that entanglement levels in the Kitaev spin-liquid phase are degenerate forming pairs, but those in the magnetically ordered phases are nondegenerate. The Schmidt gap defined as the energy difference between the lowest two levels changes at the phase boundary adjacent to the Kitaev spin-liquid phase. However, we find that phase boundaries between magnetically ordered phases do not necessarily agree with the change of the Schmidt gap.

DOI: 10.1103/PhysRevB.91.054401 PACS number(s): 75.10.Jm, 75.10.Kt, 75.25.Dk, 03.67.Mn

I. INTRODUCTION

The Kitaev honeycomb lattice model is a spin-1/2 system on a honeycomb lattice [1]. The interactions between nearest neighbors are of S^xS^x, S^yS^y, or S^zS^z type, depending on the bonds $\mathcal{J}_x$, $\mathcal{J}_y$, and $\mathcal{J}_z$, respectively, as shown in Fig. 1. The ground state of the isotropic Kitaev model is known as a gapless Kitaev spin-liquid state characterized by gapless Majorana fermion excitations with two Dirac cones [2]. The spin-spin correlation of the gapless Kitaev spin liquid is short-range, showing a nonzero value only for the nearest-neighbor sites [3]. However, perturbations such as antiferromagnetic (AFM) Heisenberg and Dzyaloskinski-Moriya interactions can qualitatively alter the nature of spin-spin correlation functions exhibiting a long-ranged power-law behavior [4].

Such a Kitaev-Heisenberg (KH) model has widely been studied as a prototype model [5] for Na_2IrO_3, and its phase diagram has been established [6–13]. We note that bond-dependent spin interactions present in the KH model have originally been studied by Kugel and Khomskii [14] on the compass model [15,16]. However, it has turned out that the KH model cannot straightforwardly explain a zigzag-type AFM order observed in Na_2IrO_3 [17,18]. This discrepancy has inspired further studies about more suitable effective spin models for Na_2IrO_3. For example, further neighbor Heisenberg interactions [17,19,20] and anisotropic interactions due to trigonal distortions [21–27] have been introduced to the KH model to explain the zigzag order. In addition, a recent neutron scattering experiment has reported that magnetic order of another iridate Li_2IrO_3 is an incommensurate spiral-type order [26,28]. It is also interesting to study such an order in the KH models extended by such interactions.

Motivated by these previous studies, we examine an extended KH model including such anisotropic interactions. We make a phase diagram of the model around the Kitaev spin-liquid phase. We find a ferromagnetic (FM) phase, a 120° AFM phase, two kinds of incommensurate (IC) phases, and a zigzag-type AFM phase next to the Kitaev spin-liquid phase. The zigzag phase exhibits spin-spin correlation similar to a model more realistic for Na_2IrO_3 [22].

Furthermore, we investigate entanglement entropy and the entanglement spectrum of the extended KH model. We find that the lowest level of the entanglement spectrum at magnetically ordered states is nondegenerate. This is clearly in contrast to the Kitaev spin-liquid state, where all of the entanglement levels form pairs. Such a degenerate structure in the Kitaev spin liquid is due to its gauge structure coming from its topological nature, and it depends on the boundary conditions. As a result, the Schmidt gap defined as the energy difference between the lowest and first excited entanglement levels changes at the phase boundary between the Kitaev spin liquid and other magnetically ordered phases. However, we find that the Schmidt gap cannot be a good measure of the phase transition between magnetically ordered phases.

This paper is organized as follows. The extended KH model and the density-matrix renormalization group (DMRG) method are introduced in Sec. II. In Sec. III, we show a phase diagram of the model around the Kitaev spin-liquid phase, obtained by the spin-spin correlation functions and the ground-state energy. The behavior of the ground-state energy, entanglement entropy, and the entanglement spectrum across phase boundaries is also shown. In addition, we discuss the entanglement spectrum of the extended KH model and clarify the relations between the Schmidt gap and the phase transition in the model. Finally, a summary and outlook are given in Sec. IV. The entanglement spectrum of the KH model is discussed in Appendix.

II. MODEL AND METHOD

The Hamiltonian of an extended KH model is given by

$$\hat{\mathcal{H}} = \sum_{\Gamma} \sum_{\langle lm \rangle \in \Gamma} \hat{\mathcal{H}}_{lm}, \tag{1}$$

*shinjo@yukawa.kyoto-u.ac.jp

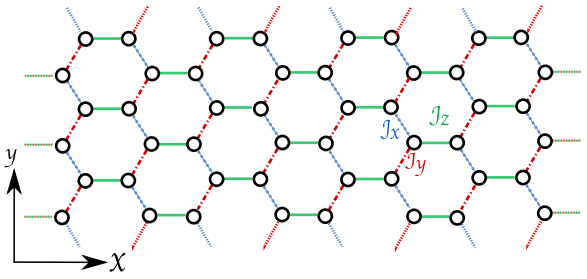

FIG. 1. (Color online) Honeycomb lattice with 6×8 sites with the periodic boundary condition. Blue dotted, red dashed-dotted, and green solid bonds labeled by $\mathcal{J}_x$, $\mathcal{J}_y$, and $\mathcal{J}_z$ have $S^x S^x$, $S^y S^y$, and $S^z S^z$ terms in a Kitaev model, respectively. We define the x-axis direction as an armchair-edge direction and the y-axis direction as a zigzag-edge direction.

$$\hat{\mathcal{H}}_{lm} = K S_l^\gamma S_m^\gamma + J\left(S_l^\alpha S_m^\alpha + S_l^\beta S_m^\beta\right) + I_1\left(S_l^\alpha S_m^\beta + S_l^\beta S_m^\alpha\right) + I_2\left(S_l^\alpha S_m^\gamma + S_l^\gamma S_m^\alpha + S_l^\beta S_m^\gamma + S_l^\gamma S_m^\beta\right), \quad (2)$$

where Γ represents a combination of $(\alpha,\beta,\gamma) = (x,y,z)$, (z,x,y), and (y,z,x) on the $\mathcal{J}_z$, $\mathcal{J}_y$, and $\mathcal{J}_x$ bonds, respectively, and $\langle lm \rangle$ sums over all possible bonds belonging to Γ. We note that I_1 and I_2 terms are added to a KH model consisting of the K and J terms. The I_1 term mainly originates from a feature of an edge-shared octahedron with total angular momentum $j = 1/2$, and the I_2 term originates mainly from trigonal distortions present in Na_2IrO_3. This model (1) has been studied by Rau and Kee [24] as an effective model describing Na_2IrO_3.

We calculate the ground state of this model by using the DMRG method [29,30]. The DMRG calculations are carried out under periodic boundary conditions. We take the x-axis direction along an armchair-edge direction and the y-axis direction along a zigzag-edge direction, as shown in Fig. 1. Unless otherwise noted, we use a system with 6 (along the y axis) $\times$ 8 (along the x axis) sites, i.e., a 48-site system. To perform DMRG, we construct a snakelike one-dimensional chain by combining the eight zigzag lines along the y axis, leading to a spin chain with long-range interactions. We keep 1000 states in the DMRG block and performed more than 10 sweeps, resulting in a typical truncation error 5×10^{-6} or smaller.

III. CALCULATED RESULTS AND DISCUSSIONS

Putting $I_1 = I_2 = 0$ into the extended KH model (1) leads to the KH model, whose phase diagram has been established [6–13]. In the phase diagram, a Kitaev spin-liquid phase emerges in the range of $K/J \leqslant -11$, when $K < 0$ and $J > 0$. An interesting issue of the extended KH model concerning Na_2IrO_3 is to find a zigzag-type AFM phase around the Kitaev spin-liquid phase [24]. Since the zigzag-type AFM phase is next to the Kitaev spin-liquid phase in the parameter region of $K < 0$ and $J > 0$, we use these signs in the present paper. It is also interesting to investigate the $K > 0$ and $J < 0$ region, but this will be a future issue.

Fixing $K/J = -25$, we find a zigzag-type AFM phase next to the Kitaev spin-liquid phase when $I_1/J > 0$ and $I_2/J < 0$, as shown in Fig. 2. The presence of the zigzag state is confirmed by examining the spin-spin correlation functions

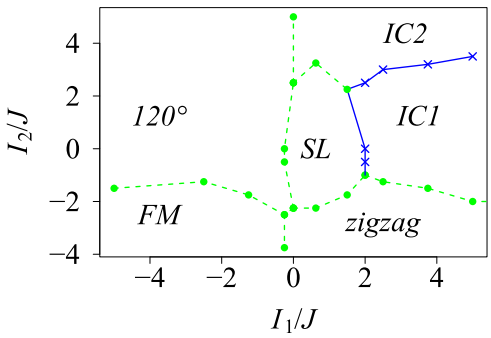

FIG. 2. (Color online) Phase diagram of the extended KH model (1). There are a ferromagnetic phase (FM), a 120° AFM phase (120°), a Kitaev spin-liquid phase (SL), two incommensurate phases (IC1, IC2), and a zigzag-type antiferromagnetic phase (zigzag). The circle and $\times$ points are determined by the second derivative of energy with respect to I_2 and connected by lines. The boundaries denoted by blue solid lines are expected to be of first-order transition, and those by green broken lines to be of continuous transition.

for each component between sites i and j, given by $\langle S_i^x S_j^x \rangle = \langle 0|\hat{S}_i^x \hat{S}_j^x|0\rangle$, $\langle S_i^y S_j^y \rangle = \langle 0|\hat{S}_i^y \hat{S}_j^y|0\rangle$, and $\langle S_i^z S_j^z \rangle = \langle 0|\hat{S}_i^z \hat{S}_j^z|0\rangle$, where $|0\rangle$ is the ground-state wave function. Figure 3 shows the calculated spin-spin correlation functions for the 48-site cluster at $I_1/J = 3.8$ and $I_2/J = -3.8$ in the zigzag phase. In the figure, the i site is indicated by a brown rhombus point. Upward red arrows and downward blue arrows denote positive and negative values of spin-spin correlation, respectively. The length of the arrows shows the absolute value of spin-spin correlation. We find the same sign within the zigzag line along the y direction in both $\langle S_i^x S_j^x \rangle$ [Fig. 3(a)] and $\langle S_i^y S_j^y \rangle$ [Fig. 3(b)], indicating the presence of the zigzag order. We note that $\langle S_i^z S_j^z \rangle$ is very short-range.

It is interesting to examine whether the zigzag phase was smoothly connected to that obtained by a more realistic effective spin model for Na_2IrO_3. Very recently, Yamaji *et al.* proposed such a model based on the electronic states obtained by the first-principles calculation [22]. By performing DMRG calculations, we have confirmed that the zigzag AFM phase in the effective model [22] exhibits spin-spin correlation similar to that shown in Fig. 3 and a similar value of the nearest neighbor spin-spin correlations. In addition, by changing parameters continuously, we have checked that there is no phase transition between the zigzag phases of the effective model and our extended KH model. Therefore, we can say that the zigzag phase in the effective model is smoothly connected to the zigzag phase in Fig. 2.

In addition to the zigzag phase, we find various magnetic phases surrounding the Kitaev spin liquid in Fig. 2, which is similar to the results obtained by classical analysis and exact diagonalization calculations [22]. In the following, we discuss the details of each phase and phase boundaries.

First, we examine the case in which $I_1/J = 0.63$. With increasing I_2, the zigzag-type AFM phase changes to an incommensurate phase denoted by IC2 through the Kitaev spin-liquid phase. Figure 4(a) shows the ground-state energy E per site. The second derivative of E with respect to I_2 is shown in Fig. 4(b). We can define phase transition points from the second derivative. At $I_2/J = -2.2$, the zigzag phase

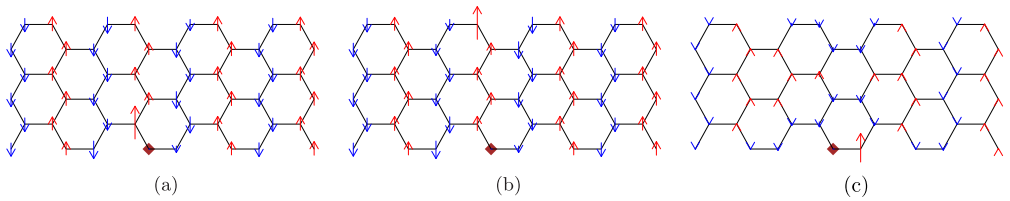

FIG. 3. (Color online) (a) $\langle S_i^x S_j^x \rangle$, (b) $\langle S_i^y S_j^y \rangle$, and (c) $\langle S_i^z S_j^z \rangle$ for zigzag-type AFM phase at $I_1/J = 3.8$ and $I_2/J = -3.8$. The i site is indicated by a brown rhombus point. Upward red arrows and downward blue arrows show positive and negative values of spin-spin correlation, respectively. The length of the arrows represents the strength of spin-spin correlation.

changes to the spin-liquid phase. The transition seems to be continuous, i.e., of second order. However, there remains a possibility that it will be of weak first order. To confirm this, we need to examine the energy profile in mode detail. This remains a future problem.

With further increasing I_2, the spin-liquid phase changes another phase at $I_2/J = 3.1$. The spin-spin correlation of the phase is shown in Figs. 5(a)–5(c). The correlations of the x and y spin components show the same sign for all sites, but the z component exhibits a different behavior, where the sign depends on the distance from the i site. This implies the presence of an incommensurate spin-spin correlation. We cannot clarify its propagation vector, since the system size we use is too small to determine it. We denote this phase as IC2.

Entanglement of the wave function can provide useful information on quantum states. It is measured by entanglement entropy and the entanglement spectrum [31]. In a system composed of two subsystems A and B, a Schmidt decomposition of a many-body state $|\psi\rangle$ reads

$$|\psi\rangle = \sum_i p_i \left|\psi_A^i\right\rangle \left|\psi_B^i\right\rangle = \sum_i e^{-\xi_i} \left|\psi_A^i\right\rangle \left|\psi_B^i\right\rangle, \tag{3}$$

where p_i is the eigenvalue of the reduced density matrix $\rho_A = \mathrm{Tr}_B |\psi\rangle\langle\psi| = e^{-\mathcal{H}_E}$ for subsystem A (or $\rho_B = \mathrm{Tr}_A |\psi\rangle\langle\psi|$ for subsystem B). The distribution of ξ_i is called the entanglement spectrum, where ξ_i is the eigenvalue of entanglement Hamiltonian $\mathcal{H}_E$. Then, von Neumann entanglement entropy containing nonlocal topological properties can be written as

$$S_{\mathrm{E}} = -\sum_i p_i \ln p_i = \sum_i \xi_i e^{-\xi_i}. \tag{4}$$

We take the A subsystem be half of the whole system throughout this paper. When we consider a system with toroidal geometry coming from periodic boundary conditions, we cut the whole system twice. In cylindrical geometry, we divide a system into two subsystems.

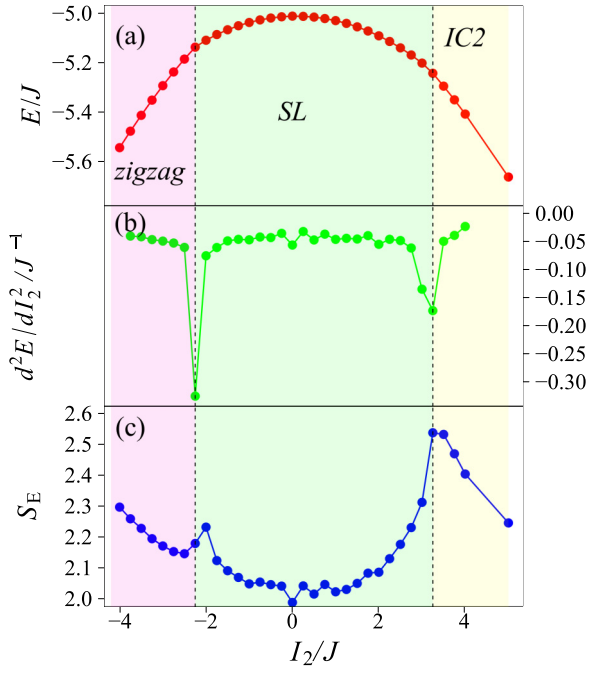

FIG. 4. (Color online) (a) The ground-state energy per site, E (red plots), (b) second derivative of E with respect to I_2, d^2E/dI_2^2 (green plots), and (c) entanglement entropy (blue plots). $I_1/J = 0.63$. The vertical dotted lines denote the phase boundary determined by the second derivative of E.

In Fig. 4(c), S_{E} for $I_1/J = 0.63$ is shown. S_{E} shows a peak structure near the phase boundary, but the peak position is not exactly at the boundary. This is clearly seen at $I_2/J \simeq -2$, where there is a boundary between the zigzag and spin-liquid phases. There have been many studies about the relationship between entanglement entropy and the phase transition in one-dimensional systems [32,33], showing a diverging behavior in S_{E} at phase transition points. However, such a relationship has not yet been established in two-dimensional systems. Therefore, we need to make clear whether the relationship is applicable for our system or not. For this purpose, the entanglement spectrum may be helpful for understanding the behavior of entanglement entropy at the phase boundary.

Before discussing the entanglement spectrum near the phase boundary, we show the spectrum for a zigzag-type ordered state ($I_1/J = 3.8$ and $I_2/J = -3.8$) in Fig. 6, where entanglement levels are plotted from the smallest value starting from $i = 1$. The lowest level of the entanglement spectrum ξ_1 is nondegenerate and separated from ξ_2. In the following, we call the level separation ξ_2-ξ_1 the Schmidt gap. We note that the nondegenerate ξ_1 is clearly in contrast to the Kitaev spin-liquid state, where all of the entanglement levels form pairs (see Appendix).

The spectral distribution of the entanglement spectrum changes with changing parameters. Figure 7 shows the entanglement spectrum for the $I_1 = 0.63$ case corresponding to Fig. 4. We find that the Schmidt gap changes from zero to finite at $I_2/J = -2.2$ ($I_2/J = 3.2$) with decreasing (increasing) I_2 from the spin-liquid phase. These I_2 values are consistent with the transition points obtained by the second derivative of E.

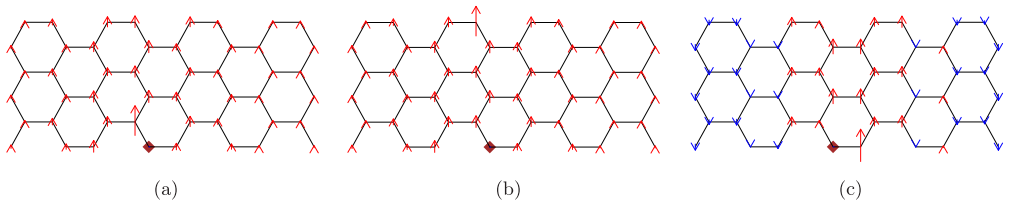

FIG. 5. (Color online) (a) $\langle S_i^x S_j^x \rangle$, (b) $\langle S_i^y S_j^y \rangle$, and (c) $\langle S_i^z S_j^z \rangle$ for the IC2 phase at $I_1/J = 2.5$ and $I_2/J = 5.0$. The i site is indicated by a brown rhombus point. Upward red arrows and downward blue arrows show positive and negative values of spin-spin correlation, respectively. The length of the arrows represents the strength of spin-spin correlation.

Comparing $I_2/J = -2.2$ with the peak position of $S_{\rm E}$ ($I_2/J = -2.0$), we may judge that the Schmidt gap is more appropriate than the entanglement entropy for the determination of the phase boundary in two-dimensional systems. Of course, more studies on different systems are necessary to confirm this statement. We also note that there is a different case in which the Schmidt gap itself cannot be a measure of the phase transition, as will be discussed below.

Here, we comment on the degeneracy of ξ_i in the Kitaev spin-liquid phase, which is located at the middle region of Fig. 7. $[n]$ in this figure shows the number of degeneracy of the lowest entanglement level, and [4] in the Kitaev spin-liquid phase denotes fourfold degeneracy. As discussed in Appendix, this is due to the gauge structure of the Kitaev spin liquid. We consider that the degeneracy is one of the "fingerprints" of the Kitaev spin liquid. Such a gauge structure also appears in topological entanglement entropy [34], and thus the degeneracy of the entanglement spectrum is useful for characterizing the nature of the spin-liquid phase. We discuss the entanglement spectrum of the Kitaev spin liquid in more detail in Appendix.

Returning to the phase diagram in Fig. 2, we next examine the case in which $I_1/J = 3.8$. Figures 8(a) and 8(b) show E and d^2E/dI_2^2, respectively. With increasing I_2, the zigzag-type AFM phase changes to the IC2 phase through a new phase denoted by IC1. The second derivative of E indicates that the phase transition between the zigzag and IC1 phases at $I_2/J = -1.5$ is of continuous order, and that between the IC1 and IC2 phases at $I_2/J = 3.2$ is of first order. Spin-spin correlation functions in the IC1 phase are shown in Figs. 9(a), 9(b), and 9(c) for $\langle S_i^x S_j^x \rangle$, $\langle S_i^y S_j^y \rangle$, and $\langle S_i^z S_j^z \rangle$, respectively. $\langle S_i^x S_j^x \rangle$ and $\langle S_i^y S_j^y \rangle$ indicate a noncommensurate spin arrangement, though $\langle S_i^z S_j^z \rangle$ shows a FM correlation. This pattern of the spin-spin correlation is different from that in IC2 shown in Fig. 5. Therefore, we denote this phase as IC1.

The sudden change of $S_{\rm E}$ at $I_2/J = 3.2$ in Fig. 8(c) is consistent with the first-order transition. The entanglement spectrum and the Schmidt gap also show a change at the same value, as shown in Fig. 10. On the other hand, the phase boundary at $I_2/J = -1.5$ disagrees with the peak position of $S_{\rm E}$ and also disagrees with the change of the Schmidt gap. Such a disagreement is different from the case of the boundary between the zigzag and spin-liquid phases discussed above.

Thirdly, let us examine the case of $I_1/J = -1.3$. Figures 11(a), 11(b), and 11(c) show E, d^2E/dI_2^2, and $S_{\rm E}$, respectively. With increasing I_2, phase changes from a FM phase to a 120° phase at $I_2/J = -1.8$ with continuous transition. This 120° phase has the same spin configuration as presented by Rau and Kee [23,24]. Entanglement entropy smoothly changes at the phase boundary, in contrast to other cases in which a peak structure appears.

Figure 12 shows the entanglement spectrum as a function of I_2. We find that the Schmidt gap changes from zero to finite at $I_2/J = -2.8$, but there is no qualitative change at the phase boundary $I_2/J = -1.8$. This means that the Schmidt

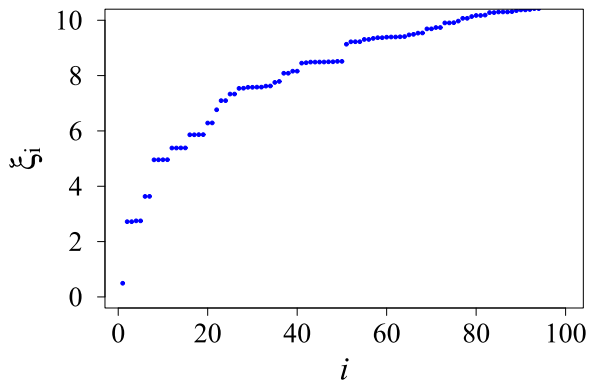

FIG. 6. (Color online) Entanglement spectrum for a zigzag-type AFM ordered ground state at $I_1/J = 3.8$ and $I_2/J = -3.8$.

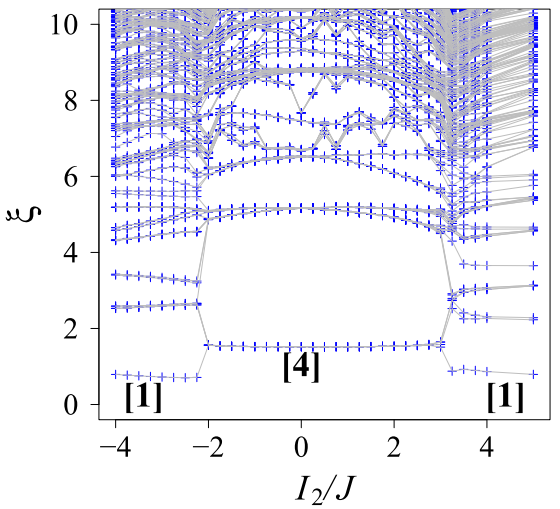

FIG. 7. (Color online) Entanglement spectrum for the extended KH model (1). $I_1/J = 0.63$. Blue crosses represent entanglement levels and gray lines connect the spectrum belonging to the same entanglement levels. $[n]$ denotes n-fold degeneracy of the lowest entanglement level in each phase.

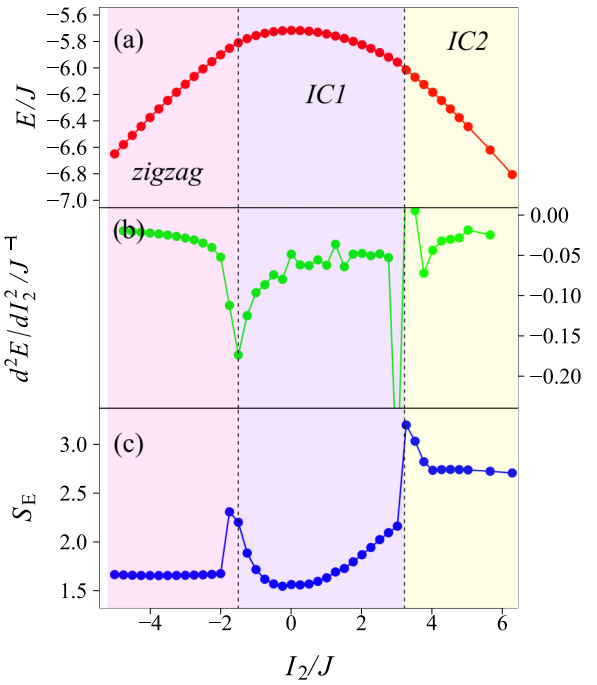

FIG. 8. (Color online) Same as Fig. 4, but $I_1/J = 3.8$.

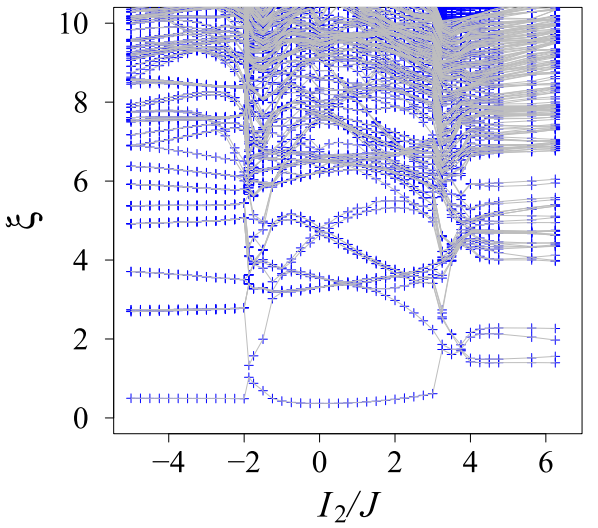

FIG. 10. (Color online) Same as Fig. 7, but $I_1/J = 3.8$.

gap is not a good measure of the phase transition in this case, where the FM phase changes to the 120° AFM phase. Recently, it has been shown that the low-energy entanglement spectrum can exhibit singular changes, even when the physical system remains in the same phase [35], suggesting less universal information about quantum phases in the low-energy entanglement spectrum.

Therefore, we can say that our case would be such an example in two-dimensional systems, where the Schmidt gap cannot characterize the phase transition points.

IV. SUMMARY AND OUTLOOK

We have studied the extended KH model (1) by using DMRG and constructed a phase diagram around the Kitaev spin-liquid phase. We have found a FM phase, a 120° phase, two kinds of incommensurate phases (IC1 and IC2), and a zigzag-type AFM phase next to the Kitaev spin-liquid phase. The zigzag phase exhibits spin-spin correlation similar to a more realistic model for Na_2IrO_3 [22]. We define phase boundaries by using the second derivative of energy. At the boundaries, entanglement entropy does not necessarily show an anomalous behavior. This means that the entanglement entropy is not a good measure for determining the phase boundary in the extended KH model.

Examining the entanglement spectrum, we have found that the lowest entanglement level in magnetically ordered states is nondegenerate. This is in contrast to that of the Kitaev spin-liquid phase, where all of entanglement levels form pairs. We note that the degeneracy in Kitaev spin liquid is due to the gauge structure, and the number of its degeneracy depends on the boundary condition reflecting the topological nature of the Kitaev spin liquid, as discussed in Appendix. Therefore, the phase boundaries between the Kitaev spin liquid and the magnetically ordered phases are determined by examining the entanglement spectrum. In this case, the Schmidt gap, defined as the difference between the lowest and first-excited entanglement levels, is a useful quantity to determine the boundary.

However, as far as phase transitions between magnetically ordered phases are concerned, we have found that the Schmidt gap is not necessarily a measure of phase transition. For example, the Schmidt gap cannot characterize the phase transition between the FM and the 120° AFM phases, between zigzag-type AFM and IC1 phases, and between the IC1 and IC2 phases.

In one-dimensional quantum many-body systems, the Schmidt gap is known to be a novel quantity for identifying and characterizing various phases and phase transitions. In two-dimensional systems, however, the meaning of the Schmidt gap has not yet been clarified as far as we know. Therefore, we consider that the present work will provide a starting point for the study of the relation between the entanglement spectrum and the quantum state in two dimensions. In fact, our present study of the entanglement spectrum is closely

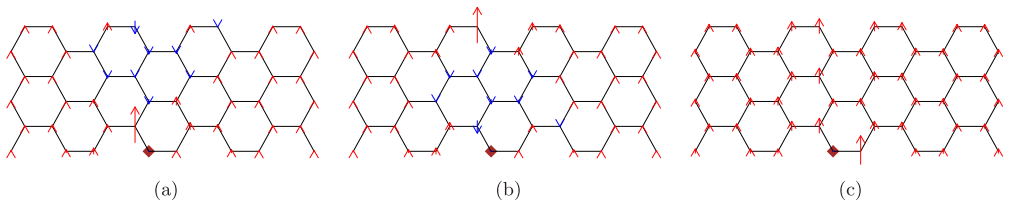

FIG. 9. (Color online) Same as Fig. 5, but for the IC1 phase at $I_1/J = 2.5$ and $I_2/J = 2.5$.

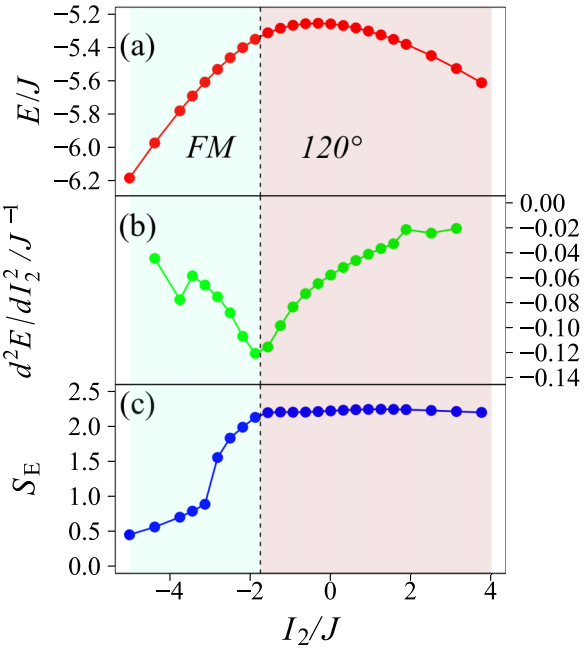

FIG. 11. (Color online) Same as Fig. 4, but $I_1/J = -1.3$.

related to other studies attempting unbiasedly to detect order parameters and/or dominant correlations using reduced density matrices [36,37]. We believe that we are able to extract much more information from the structure of entanglement and to identify and characterize various orders more efficiently, once we understand the nature of entanglement in many-body interacting systems.

ACKNOWLEDGMENTS

We acknowledge Y. Yamaji, S. Morita, M. Kurita, M. Imada, T. Okubo, N. Kawashima, K. Totsuka, and S. Yunoki for useful and stimulating discussions. This work is financially supported by MEXT HPCI Strategic Programs for Innovative Research (SPIRE) (hp130007, hp140215, hp140136) and the Computational Materials Science Initiative (CMSI). Numerical calculation was partly carried out at the K computer, the RIKEN Advanced Institute for Computational Science, and the Supercomputer Center, Institute for Solid State Physics, University of Tokyo. This work was also supported by Grants-in-Aid for Scientific Research (No. 26287079 and No. 22740225) from MEXT, Japan.

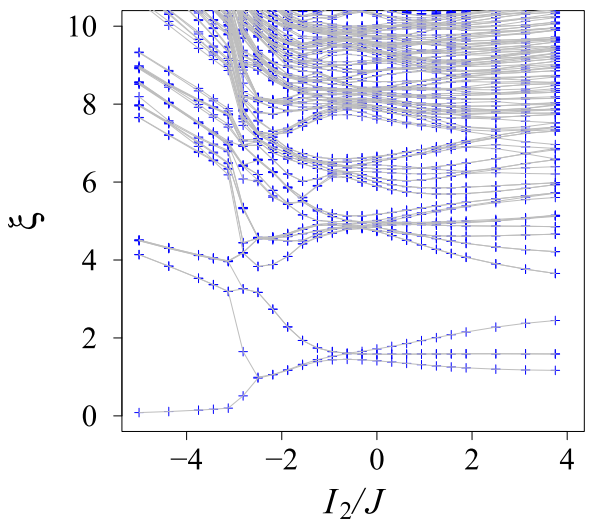

FIG. 12. (Color online) Same as Fig. 7, but $I_1/J = -1.3$.

APPENDIX: ENTANGLEMENT SPECTRUM

Li and Haldane proposed an entanglement spectrum that contains the full set of eigenvalues of the density matrix [31]. Writing the eigenvalues of the density matrix as $e^{-\xi_i}$, where ξ_i is an entanglement level, they showed that the low-level entanglement spectrum for Laughlin, Moore-Read, and Read-Rezayi states exhibits a universal structure related to the associated conformal field theory. The universal structure is separated from a nonuniversal high-level spectrum by an entanglement gap that is finite in the thermodynamic limit. This gap is proposed to be a "fingerprint" of the topological order. Since the proposal, the entanglement spectrum has been studied in various systems, including fractional quantum Hall systems [31,38–40], topological insulators [41,42], spin chains [43], and the Kitaev honeycomb lattice model [34]. Furthermore, it has been realized that the scaling of the Schmidt gap defined by the difference between the two largest eigenvalues of the reduced density matrix is useful for detecting critical points through studies of the one-dimensional Kugel-Khomskii model [44], spin chains [45,46], and the two-dimensional quantum Ising model [47]. The entanglement spectrum is thus now accepted to be a quantity characterizing not only various phases but also phase transitions. However, it was recently pointed out that the low-energy entanglement spectrum does not necessarily provide universal information about quantum phases [35]. Therefore, it is interesting to examine the entanglement spectrum of the KH model, whose ground state is well known [6].

1. Kitaev-Heisenberg model

In this section, we defined the KH model as

$$\mathcal{H} = \sum_{\langle i,j \rangle} \left[-2\alpha S_i^\gamma S_j^\gamma + (1-\alpha) \boldsymbol{S}_i \cdot \boldsymbol{S}_j \right], \qquad \text{(A1)}$$

where α is related to K and J in Eq. (1) as $J = 1 - \alpha$ and $K = 1 - 3\alpha$. The ground state at $\alpha = 0$ and 1 is the Néel and Kitaev spin-liquid state, respectively. In between, there is a stripy-type AFM state.

Figure 13 shows the entanglement spectrum of the 6×8-site KH model with periodic boundary conditions as a function of α. Hereafter, we call the periodic boundary condition the toroidal boundary condition. We find that the level structure changes at $\alpha \simeq 0.4$ and $\alpha \simeq 0.86$. These values are consistent with phase transition points determined by the second derivative of energy with respect to α.

We find that the Kitaev spin-liquid phase exhibits fourfold degeneracy in the ground state, while the Néel and stripy phases show the nondegenerate lowest energy level. The degeneracy of the spin-liquid phase comes from its gauge structure, as will be discussed in Appendix 2.

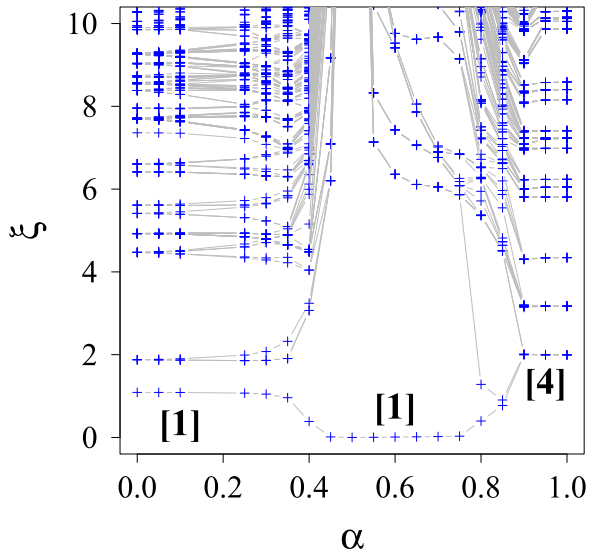

FIG. 13. (Color online) The entanglement spectrum for the KH model (A1). Blue crosses represent entanglement levels and gray lines connect the spectrum belonging to the same entanglement levels. $[n]$ denotes n-fold degeneracy of the lowest entanglement level in each phase.

The Schmidt gap increases drastically at $\alpha \simeq 0.4$ with increasing α. This indicates that a phase transition occurs there. At the exactly solvable point $\alpha = 0.5$, the gap diverges, since the ground state can be written by a single product state. With further increasing α, the Schmidt gap closes between $\alpha = 0.85$ and 9.0. This is again consistent with the position of the phase boundary. Of course, in order to determine the phase boundary precisely, it is important to study finite-size scaling of the Schmidt gap.

2. Kitaev spin-liquid state

In this section, we discuss the dependence of the entanglement spectrum in the Kitaev spin-liquid state on the system size and the boundary condition. First of all, we consider the degeneracy of the entanglement spectrum for a $6 \times L_x$ ($L_x \to \infty$) system by counting the Wilson loops that are cut when the whole system is divided into two subsystems [1,48,49]. In our cluster configuration, it is inevitable to have two Wilson loops, for example W_1 and W_2 defined on two neighboring hexagons, as shown in Fig. 14. The two loops induce twofold degeneracy. The number of degeneracy increases as the number of Wilson loops defined on the honeycomb lattice increases. We can define more Wilson loops in the toroidal boundary condition than in the cylindrical boundary condition.

Let us briefly confirm this. Figure 14 shows a 6×8-site system, where the number labels sites on the honeycomb lattice and vertical lines denote the cutting position when we divide the whole system into two subsystems to calculate the entanglement spectrum. Note that a system with the toroidal boundary condition is cut twice at a middle vertical line and a right or left line, while a system with the cylindrical boundary condition is cut only once at the middle vertical line. First, we consider the case of the cylindrical boundary condition. Then, the system is divided into A and B parts. We define the Wilson

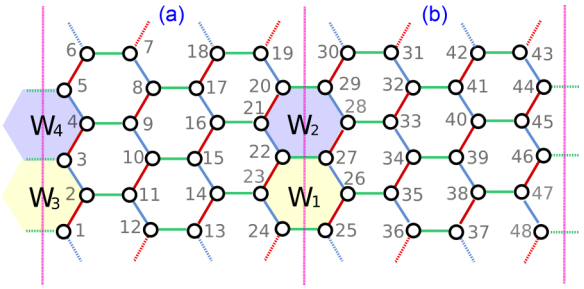

FIG. 14. (Color online) Cluster configuration of 6×8 sites. The numbers label sites on a honeycomb lattice. Vertical dashed lines denote the cutting position when we divide the whole system into two subsystems, A and B. For the cylindrical boundary condition the system is divided only once at the middle vertical line, while for the toroidal boundary condition the system is cut twice at the middle vertical line and the right or left vertical line. W_1 and W_2 show the Wilson loops defined on a hexagon on a honeycomb lattice, which crosses the middle vertical line. W_3 and W_4 show the loops that cross the right or left vertical line.

loops as

$$\hat{W}_1 = \hat{\sigma}^y_{24}\hat{\sigma}^z_{23}\hat{\sigma}^x_{22}\hat{\sigma}^y_{27}\hat{\sigma}^z_{26}\hat{\sigma}^x_{25} = \hat{w}^A_1\hat{w}^B_1,$$
$$\hat{W}_2 = \hat{\sigma}^y_{22}\hat{\sigma}^z_{21}\hat{\sigma}^x_{20}\hat{\sigma}^y_{29}\hat{\sigma}^z_{28}\hat{\sigma}^x_{27} = \hat{w}^A_2\hat{w}^B_2,$$

where σ^x_i, σ^y_i, and σ^z_i are Pauli matrices at the i site, and

$$\hat{w}^A_1 = \hat{\sigma}^y_{24}\hat{\sigma}^z_{23}\hat{\sigma}^x_{22}, \quad \hat{w}^B_1 = \hat{\sigma}^y_{27}\hat{\sigma}^z_{26}\hat{\sigma}^x_{25},$$
$$\hat{w}^A_2 = \hat{\sigma}^y_{22}\hat{\sigma}^z_{21}\hat{\sigma}^x_{20}, \quad \hat{w}^B_2 = \hat{\sigma}^y_{29}\hat{\sigma}^z_{28}\hat{\sigma}^x_{27}.$$

Note that the commutation relation

$$\left[\hat{W}_1, \hat{W}_2\right] = 0 \tag{A2}$$

and the anticommutation relations

$$\left\{\hat{w}^A_1, \hat{w}^A_2\right\} = 0, \quad \left\{\hat{w}^B_1, \hat{w}^B_2\right\} = 0.$$

The ground state is a vortex-free state, so that the ground state should be an eigenstate of $\hat{W}_1$ with eigenvalue $+1$:

$$\hat{W}_1|\psi\rangle = +|\psi\rangle.$$

The ground state can be written as

$$|\psi\rangle = |W_1 = +1\rangle \tag{A3}$$
$$= c_+\left|w^A_1 = +1, w^B_1 = +1\right\rangle + c_-\left|w^A_1 = -1, w^B_1 = -1\right\rangle, \tag{A4}$$

with

$$\hat{w}^{A,B}_1\left|w^{A,B}_1 = \pm 1\right\rangle = \pm\left|w^{A,B}_1 = \pm 1\right\rangle.$$

The eigenstates obey

$$\hat{w}^A_2\left|w^A_1 = +1\right\rangle = \left|w^A_1 = -1\right\rangle,$$
$$\hat{w}^A_2\left|w^A_1 = -1\right\rangle = \left|w^A_1 = +1\right\rangle.$$

Furthermore, from Eq. (A2), the ground state $|\psi\rangle$ is a simultaneous eigenstate of W_1 and W_2, so that $|\psi\rangle$ is also

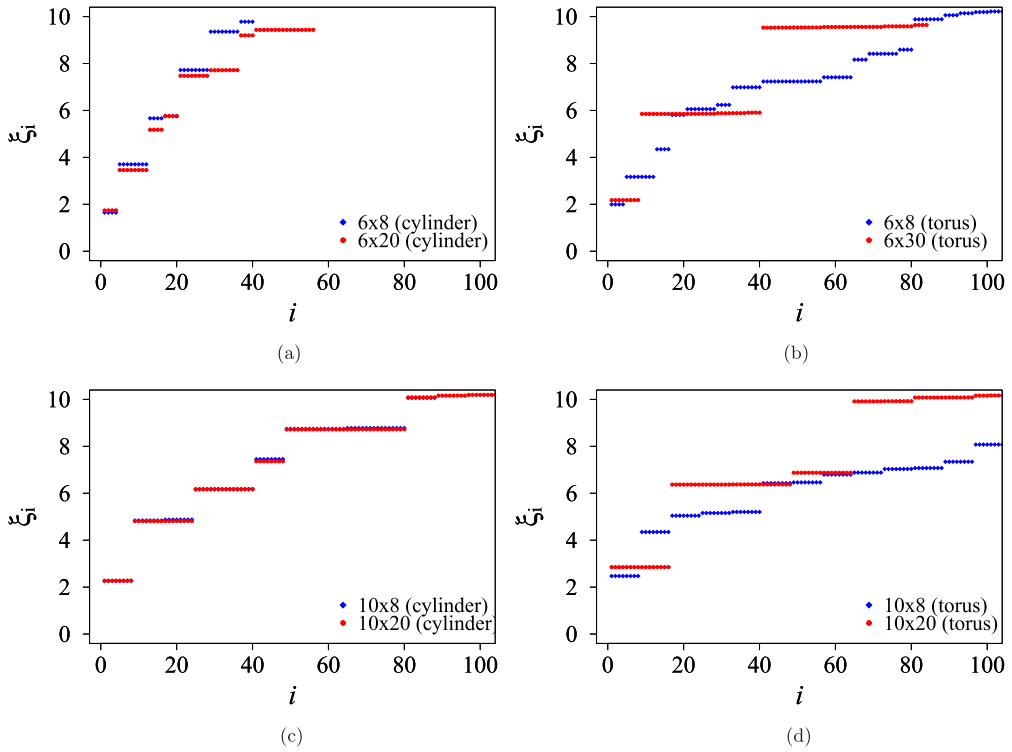

FIG. 15. (Color online) The dependence of the entanglement spectrum ξ_i of the Kitaev spin liquid on system size and boundary condition. (a) 6×8-site system (blue rhombuses) and 6×20-site system (red circles) with the cylindrical boundary condition, (b) 6×8-site system (blue rhombuses) and 6×30-site system (red circles) with the toroidal boundary condition, (c) 10×8-site system (blue rhombuses) and 10×20-site system (red circles) with the cylindrical boundary condition, and (d)10×8-site system (blue rhombuses) and 10×20-site system (red circles) with the toroidal boundary condition.

an eigenstate of W_2:

$$\begin{aligned}\hat{W}_2|\psi\rangle &= \hat{w}_2^A\hat{w}_2^B|W_1=+1\rangle \\ &= c_+\hat{w}_2^A\hat{w}_2^B\left|w_1^A=+1,w_1^B=+1\right\rangle \\ &\quad + c_-\hat{w}_2^A\hat{w}_2^B\left|w_1^A=-1,w_1^B=-1\right\rangle \\ &= c_+\left|w_1^A=-1,w_1^B=-1\right\rangle \\ &\quad + c_-\left|w_1^A=+1,w_1^B=+1\right\rangle \\ &= +|\psi\rangle. \end{aligned} \tag{A5}$$

Therefore, comparing Eq. (A4) and Eq. (A5), we obtain

$$c_+ = c_- \equiv c$$

and

$$|\psi\rangle = c\left(\left|w_1^A=+1,w_1^B=+1\right\rangle + \left|w_1^A=-1,w_1^B=-1\right\rangle\right).$$

The reduced density matrix of subsystem A reads

$$\begin{aligned}\rho_A &= \mathrm{Tr}_B\rho = \mathrm{Tr}_B|\psi\rangle\langle\psi| \\ &= \left\langle w_1^B=1\right|\rho\left|w_1^B=1\right\rangle + \left\langle w_1^B=-1\right|\rho\left|w_1^B=-1\right\rangle \\ &= c\left(\left|w_1^A=+1\right\rangle\left\langle w_1^A=+1\right| + \left|w_1^A=-1\right\rangle\left\langle w_1^A=-1\right|\right) \\ &= c\begin{pmatrix}1 & 0\\ 0 & 1\end{pmatrix}.\end{aligned}$$

Therefore, we find that the eigenvalues of ρ_A, i.e., entanglement spectra, are twofold-degenerate.

It is possible to define the third Wilson loop above W_2, which shares the 24-25 (20-29) edge with the W_1 (W_2) loop. However, the same procedure as (A5) with respect to the third loop will give a result similar to the case of W_2. This means no additional state for ρ_A, and thus the third loop does not contribute to increasing the number of degeneracy.

Next, we consider a system with the toroidal boundary condition in a similar way. In this case, we define additional Wilson loops W_3 and W_4 that are located on the pink line at the edge of Fig. 14. These Wilson loops contribute to additional degeneracy of the entanglement spectrum, resulting in 2^2-fold degeneracy of the entanglement spectrum. A similar result to this discussion was obtained by Yao and Qi [34], where the number of degeneracy of the entanglement spectrum is 2^{L-1}, with L being the length of the boundary between the A and B subsystems.

Based on the discussion above, we expect that the number of degeneracy in a $10 \times L_x$-site system is larger than that in a $6 \times L_x$-site system, since the length of the boundary between A and B is longer, i.e., the number of Wilson loops defined on a honeycomb lattice is larger in the former than in the latter. We confirm this by our DMRG calculations as shown in Fig. 15, where we kept 700 states in the DMRG block and performed more than 20 sweeps, resulting in a truncation error 10^{-10} or smaller.

Blue rhombuses and red circles in Fig. 15(a) show low entanglement levels for cylindrical 6×8-site and 6×20-site systems, respectively. We find that the levels are at least fourfold-degenerate. The results for the same system but with

the toroidal boundary condition are shown in Fig. 15(b), where, in contrast with the cylindrical boundary condition, the number of degeneracy strongly depends on the system size along the x-axis direction: at least fourfold degeneracy for the 6×8-site system and at least eightfold degeneracy for the 6×30-site system. We also examined 6×12-site and 6×20-site systems and obtained the same result (not shown). Therefore, we can conclude that there is fourfold degeneracy for $6 \times L_x$ with the cylindrical boundary condition and eightfold with the toroidal boundary condition, as discussed above.

Next, we enlarge the system along the y-axis direction. Blue rhombuses and red circles in Fig. 15(c) show low entanglement levels for the cylindrical 10×8-site and 10×20-site systems, respectively. We find that the levels are at least eightfold degenerate and thus the degeneracy is doubled as compared with the $6 \times L_x$-site system. The results for the same system but with the toroidal boundary condition are shown in Fig. 15(d), where, in contrast with the cylindrical boundary condition, the number of degeneracy strongly depends on the system size along the y-axis direction: at least eightfold degeneracy for the 10×8-site system and at least 16-fold degeneracy for the 10×20-site system. Therefore, we can conclude that there is eightfold degeneracy for $10 \times L_x$ with the cylindrical boundary condition and 16-fold with the toroidal boundary condition. All of these numerical results are consistent with the analytical ones mentioned above.

The ground state of the Kitaev spin-liquid state can be regarded as Majorana fermions coupled with the $\mathbb{Z}_2$ gauge field. The gauge field is, thus, the origin of the degeneracy of the entanglement spectrum. We note that such a gauge fluctuation also affects topological entanglement entropy [34].

[1] A. Kitaev, Ann. Phys. (NY) **321**, 2 (2006).
[2] J. Knolle, D. L. Kovrizhin, J. T. Chalker, and R. Moessner, Phys. Rev. Lett. **112**, 207203 (2014).
[3] G. Baskaran, S. Mandal, and R. Shankar, Phys. Rev. Lett. **98**, 247201 (2007).
[4] S. Mandal, S. Bhattacharjee, K. Sengupta, R. Shankar, and G. Baskaran, Phys. Rev. B **84**, 155121 (2011).
[5] G. Jackeli and G. Khaliullin, Phys. Rev. Lett. **102**, 017205 (2009).
[6] J. Chaloupka, G. Jackeli, and G. Khaliullin, Phys. Rev. Lett. **105**, 027204 (2010).
[7] H.-C. Jiang, Z.-C. Gu, X.-L. Qi, and S. Trebst, Phys. Rev. B **83**, 245104 (2011).
[8] J. Reuther, R. Thomale, and S. Trebst, Phys. Rev. B **84**, 100406 (2011).
[9] S. Okamoto, Phys. Rev. B **87**, 064508 (2013).
[10] R. Schaffer, S. Bhattacharjee, and Y. B. Kim, Phys. Rev. B **86**, 224417 (2012).
[11] J. Chaloupka, G. Jackeli, and G. Khaliullin, Phys. Rev. Lett. **110**, 097204 (2013).
[12] C. Price and N. B. Perkins, Phys. Rev. B **88**, 024410 (2013).
[13] E. Sela, H.-C. Jiang, M. H. Gerlach, and S. Trebst, Phys. Rev. B **90**, 035113 (2014).
[14] K. Kugel and D. Khomskii, Sov. Phys. Usp. **25**, 231 (1982).
[15] G. Khaliullin, Prog. Theor. Phys. Suppl. **160**, 155 (2005).
[16] Z. Nussinov and J. van den Brink, Compass and kitaev models – theory and physical motivations, arXiv:1303.5922 [cond-mat.str-el].
[17] S. K. Choi, R. Coldea, A. N. Kolmogorov, T. Lancaster, I. I. Mazin, S. J. Blundell, P. G. Radaelli, Y. Singh, P. Gegenwart, K. R. Choi, S.-W. Cheong, P. J. Baker, C. Stock, and J. Taylor, Phys. Rev. Lett. **108**, 127204 (2012).
[18] F. Ye, S. Chi, H. Cao, B. C. Chakoumakos, J. A. Fernandez-Baca, R. Custelcean, T. F. Qi, O. B. Korneta, and G. Cao, Phys. Rev. B **85**, 180403 (2012).
[19] I. Kimchi and Y.-Z. You, Phys. Rev. B **84**, 180407 (2011).
[20] A. F. Albuquerque, D. Schwandt, B. Hetényi, S. Capponi, M. Mambrini, and A. M. Läuchli, Phys. Rev. B **84**, 024406 (2011).
[21] S. Bhattacharjee, S.-S. Lee, and Y. B. Kim, New J. Phys. **14**, 073015 (2012).
[22] Y. Yamaji, Y. Nomura, M. Kurita, R. Arita, and M. Imada, Phys. Rev. Lett. **113**, 107201 (2014).
[23] J. G. Rau, E. K.-H. Lee, and H.-Y. Kee, Phys. Rev. Lett. **112**, 077204 (2014).
[24] J. G. Rau and H.-Y. Kee, Trigonal distortion in the honeycomb iridates: Proximity of zigzag and spiral phases in Na2IrO3, arXiv:1408.4811 [cond-mat.str-el].
[25] Y. Sizyuk, C. Price, P. Wölfle, and N. B. Perkins, Phys. Rev. B **90**, 155126 (2014).
[26] I. Kimchi, R. Coldea, and A. Vishwanath, Unified theory of spiral magnetism in the harmonic-honeycomb iridates α,β,γ-Li2IrO3, arXiv:1408.3640 [cond-mat.str-el].
[27] V. M. Katukuri, S. Nishimoto, V. Yushankhai, A. Stoyanova, H. Kandpal, S. Choi, R. Coldea, I. Rousochatzakis, L. Hozoi, and J. van den Brink, New J. Phys. **16**, 013056 (2014).
[28] J. Reuther, R. Thomale, and S. Rachel, Phys. Rev. B **90**, 100405(R) (2014).
[29] S. R. White, Phys. Rev. Lett. **69**, 2863 (1992).
[30] U. Schollwöck, Rev. Mod. Phys. **77**, 259 (2005).
[31] H. Li and F. D. M. Haldane, Phys. Rev. Lett. **101**, 010504 (2008).
[32] C. Holzhey, F. Larsen, and F. Wilczek, Nucl. Phys. B **424**, 443 (1994).
[33] P. Calabrese and J. Cardy, J. Stat. Mech. (2004) P06002.
[34] H. Yao and X.-L. Qi, Phys. Rev. Lett. **105**, 080501 (2010).
[35] A. Chandran, V. Khemani, and S. L. Sondhi, Phys. Rev. Lett. **113**, 060501 (2014).
[36] S. Furukawa, G. Misguich, and M. Oshikawa, Phys. Rev. Lett. **96**, 047211 (2006).
[37] C. L. Henley and H. J. Changlani, J. Stat. Mech. (2014) P11002.
[38] N. Regnault, B. A. Bernevig, and F. D. M. Haldane, Phys. Rev. Lett. **103**, 016801 (2009).
[39] A. M. Läuchli, E. J. Bergholtz, J. Suorsa, and M. Haque, Phys. Rev. Lett. **104**, 156404 (2010).
[40] R. Thomale, A. Sterdyniak, N. Regnault, and B. A. Bernevig, Phys. Rev. Lett. **104**, 180502 (2010).
[41] A. M. Turner, Y. Zhang, and A. Vishwanath, Phys. Rev. B **82**, 241102 (2010).
[42] L. Fidkowski, Phys. Rev. Lett. **104**, 130502 (2010).

[43] R. Thomale, D. P. Arovas, and B. A. Bernevig, Phys. Rev. Lett. **105**, 116805 (2010).
[44] R. Lundgren, V. Chua, and G. A. Fiete, Phys. Rev. B **86**, 224422 (2012).
[45] L. Lepori, G. De Chiara, and A. Sanpera, Phys. Rev. B **87**, 235107 (2013).
[46] S. M. Giampaolo, S. Montangero, F. Dell'Anno, S. De Siena, and F. Illuminati, Phys. Rev. B **88**, 125142 (2013).
[47] A. J. A. James and R. M. Konik, Phys. Rev. B **87**, 241103 (2013).
[48] E. Fradkin, *Field Theories of Condensed Matter Physics* (Cambridge University Press, Cambridge, 2013).
[49] S. Morita (private communication).